2020 IEEE/RSJ International Conference on Intelligent Robots and Systems (IROS)
October 25-29, 2020, Las Vegas, NV, USA (Virtual)

Magnetically Programmable Cuboids for 2D Locomotion and Collaborative Assembly

Louis William Rogowski, Anuruddha Bhattacharjee, Xiao Zhang,
Gokhan Kararsiz, Henry C. Fu, and Min Jun Kim*

***Abstract*— The modular assembly and actuation of 3D printed milliscale cuboid robots using a globally applied magnetic field is presented. Cuboids are composed of a rectangular resin shell embedded with two spherical permanent magnets that can independently align with any applied magnetic field. Placing cuboids within short distances of each other allows for modular assembly and disassembly by changing magnetic field direction. Assembled cuboids are demonstrated to stably self-propel under sequential field inputs allowing for both rolling and pivot walking motion modes. Swarms of cuboids could be actuated within the working space and exhibit near identical behavior. Specialized 'trap robots' were developed to capture objects, transport them within the working space, and subsequently release the payload in a new location. Cuboids with male and female connectors were developed to exhibit the selective mating between cuboids. The results show that cuboids are a diverse and adaptable platform that has the potential to be scaled down to the sub-millimeter regime for use in medical or small-scale assembly applications.**

I. Introduction

Small-scale robots have been portrayed enthusiastically in the entertainment industry with movies like Big Hero 6, Transformers, G.I. Joe: The Rise of Cobra, and Innerspace captivating audiences with their fantastical feats of adaptability and resourcefulness. While much of the technology displayed is still far from reality, the idea of independent small-scale subunits forming complex structures to perform specific tasks is an idea that reverberates throughout interdisciplinary robotics research [1], [2]. Many of these modular robots take the form of cube shapes, each equipped with their own internal motors, actuators, and power supplies [3]–[5]. Many of the connections are mechanical in nature, with some involving re-tractable hooking mechanisms, male-female connectors, or permanent magnets [6]. Most of the robots themselves can behave independently and are able to maneuver themselves within their environment to create complex shapes or user specified patterns [7]–[14]. While effective, these modular robots require sophisticated electronics and servos that are often not scalable below the millimeter regime; this is highly limiting since their applications in medical techniques would be valuable [15], [16]. While external actuation has been used to manipulate some modular reconfigurable robots [17]–[20], very little has been done on reducing their complexity. Simple microrobots have been stochastically assembled using chemical functionalizations and magnetic dipole interactions [21], but can not be easily made to pattern certain configurations on demand without the use of highly complex magnetic field inputs [22], [23], although several theoretical models exist to achieve them using more complicated microrobots [24]. While impressively reconfigurable, these microrobots lack the rigidity necessary to perform certain locomotive and transport tasks.

Louis William Rogowski, Anuruddha Bhattacharjee, Xiao Zhang, Gokhan Kararsiz, and Min Jun Kim are with Southern Methodist University, Dallas, TX 75206 USA. Henry C. Fu is with the University of Utah, Salt Lake City, UT 84112 USA. *Corresponding author (email: mjkim@lyle.smu.edu).

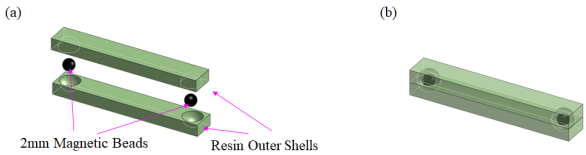

Fig. 1. (a) Exploded view and (b) fabricated cuboid robot.

Here, we present the design of a simple millimeter-sized robotic platform that can easily exhibit assembly and locomotive behavior under the influence of globally applied magnetic fields. Our cuboid robot consists of freely rotating spherical permanent magnets enclosed within rectangular 3D printed resin shells. As the externally applied magnetic field direction is changed, individual cuboids can assemble and disassemble themselves into predetermined patterns depending on their spatial locations. Assembled cuboid configurations can perform 'rolling' and 'pivot walking' motion modes to navigate through a working space. Making simple geometric changes to cuboid structures enables other interesting applications, such as object transportation and selective templating between specific cuboids. Different from other millirobots presented in the literature, the simple design of the cuboids makes them easy to scale, fabricate, and geometrically modify for specific tasks. Moreover, this modular robotic platform can turn on and off different spatial patterns of magnetic attraction and repulsion in a time-dependent manner that allows for much more flexible assembly strategies. The rest of this paper will explain the experimental setup, the results, and the future work we hope these cuboids will one day be able to accomplish.

II. Experimental Setup

A. Design and Fabrication of Cuboids

Cuboid robots were designed using an online computer-aided design software (OnShape) and printed using a stereolithography (SLA) resin printer (Anycubic Photon UV LCD 3D Printer). For easy assembly, two outer shells were printed and two spherical magnets (2 mm in diameter, Neodymium

45 of strength) were inserted inside slightly oversized hollow chambers (Fig. 1a). The two shells were then glued together using super glue to produce the completed cuboid robots (Fig. 1b). The two internal chambers housing the magnets were 3.4 mm in diameter, large enough to allow the internal magnets to rotate freely and orient themselves to any applied magnetic fields. Through experimental trial and error, it was determined that the minimal center-to-center distance for these kinds of magnets to avoid interaction with each other was 12.5 mm, thus in our configuration, we set the distance between the two magnets to be at least 22 mm from the center of each chamber to ensure that there was no interaction between magnets within the same cuboid. This separation distance is dependent on the strength of the embedded permanent magnets. The dimensions of individual cuboids used during experiments were $26{\times}4{\times}4\ mm^3$, with the minimum distance between the internal chambers and the side walls being 300 μm. Hereafter, cuboids without attachment are known as 'individual cuboids', while cuboids that are attached to other cuboids will be called 'assembled cuboids'. Other cuboid variants will be elaborated upon as they appear in subsequent sections.

B. Magnetic Field Controller

Long range magnetic fields were generated using a high powered nested Helmholtz coil system, which has been used extensively in previous work [25]. The coils were fabricated using insulated 13 gauge circular copper wire and all the support structures made up of polylactic acid (PLA) were printed by an Ultimaker 2 Extended+ 3D printer. The inner diameters of x, y, and z coils are 29.2 cm, 40.1 cm, and 20 cm, respectively. The large size of the coils allows for a total working distance of $15 \times 12 \times 8\ cm^3$ at the center of the coil configuration. Individual coil pairs were each powered by their own KEPCO BOP 50-20MG power supply; with the maximum magnetic field magnitudes produced by each coil pair able to reach above 40 mT. MATLAB was used to generate magnetic field inputs using the digital input and output toolbox. MATLAB was also used to generate trajectories from the cuboids' motions and extract instantaneous position and velocity data between individual frames. The voltage inputs were transmitted to a data acquisition board (DAQ, National Instruments) and turned into analog signals to the power supplies. The power supplies acted as a 1:5 amplifier, turning 1 volt from the DAQ board to 5 volts in the power supplies. The generalized 3D magnetic field vector (mT) produced from the system is represented by:

$$\boldsymbol{B}_G(A,\theta,\alpha) = \begin{pmatrix} A\cos(\alpha)\cos(\theta) \\ A\cos(\alpha)\sin(\theta) \\ A\sin(\alpha) \end{pmatrix}, \tag{1}$$

where A is the amplitude, θ is its angle in the x-y plane to the x axis, and α is its angle from the x-y plane. A digital camera (with 30 frame per second) was interfaced with MATLAB to record experiments and collect magnetic field settings throughout the experiments. All experiments were conducted inside a 3D printed test bed, composed entirely of PLA, and located at the center of the coil system.

C. Cuboid Interactions with Magnetic Fields

A magnetic dipole field vector $\boldsymbol{B}$ at a distance $\boldsymbol{r}$ produced from the magnetic dipole $\boldsymbol{m}$ can be described by

$$\boldsymbol{B}(\boldsymbol{r},\boldsymbol{m}) = \left(\frac{\mu_0}{4\pi\|\boldsymbol{r}\|^3}(3\boldsymbol{r}\boldsymbol{r}^T - I_3)\right)\boldsymbol{m}, \tag{2}$$

where $\mu_0 = 4\pi \times 10^{-7}\ (TmA^{-1})$ is the magnetic permeability of free space and I_3 is an identity matrix. The strength of the dipole field decays cubically with the distance $\boldsymbol{r}$ and the field is twice as strong along the axis of the dipole (i.e., $\boldsymbol{r} \parallel \boldsymbol{m}$) than the orthogonal axes to the dipole (i.e., $\boldsymbol{r} \perp \boldsymbol{m}$). The dipoles of the freely rotating magnets within the cuboids will always be aligned with the direction of a superimposed magnetic field as in Fig. 2a, where the dipoles of the individual magnets are aligned with the magnetic field oriented at an angle θ. This alignment can cause swarms of cuboids to attract or repel depending on both the direction of the applied magnetic field and the spatial configuration of other cuboids within the working space. An example of this can be seen in Fig. 2b-d, where the attraction and repulsion of four cuboid robots is presented for different magnetic field orientations: where the magnetic field is pointed along the (b) z direction; (c) x direction; and (d) y direction. Cuboid swarms needed to be within a few millimeters of each other to guarantee assembly and were manually placed in close proximity prior to experiments. The assembled cuboids generated from Fig. 2c will have shared magnetic dipoles which fix the two cuboids in place and prevent the free rotation of their individual permanent magnets. Once assembled, the dipoles no longer rotate relative to the cuboid bodies; therefore, the dipole pair will rotate the cuboid bodies to orient to the direction of the applied magnetic field. An example of body rotation is shown in Fig. 2e, where a magnetic field is slowly rotated counterclockwise in the working space. These fixed dipole pairs also allow assembled cuboids to exhibit motion modes, such as pivot walking and rolling (see Section II

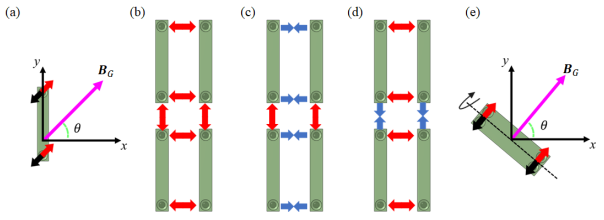

Fig. 2. (a) When a magnetic field ($\boldsymbol{B}_G$) is applied along the x-y plane at an angle θ, the magnets inside the cuboid are aligned with the magnetic field. (b) When the magnetic field is oriented along the positive or negative z direction, the cuboids repel each other. (c) When the magnetic field is oriented along the positive or negative x direction, the cuboids directly next to each other attract one another. (d) When the magnetic field is oriented along the positive or negative y direction, the cuboids above and below attract each other. Red arrows in (b-d) stand for repulsive forces, whereas blue arrows stand for attractive forces. (e) Assembled cuboids produced in (c) will fully orient their shells to align with the magnetic field at an angle θ and can rotate about the rotation axis (dashed line) without disassembling as the magnets are now fixed between them due to attraction with each other.

D) [25], while individual cuboids remain stationary. Fast rotations were found to often cause a sudden disassembly and were found to be unreliable for cuboid propulsion mechanisms (see results). There were multiple methods used to disassemble the assembled cuboids, with the most reliable method found through experimentation being to disengage the magnetic fields and then immediately point the magnetic fields in a direction perpendicular to the attached dipoles; this would cause the assembled cuboids to suddenly separate. Another disassembly method used was to suddenly switch the magnetic fields from positive to negative orientation and then quickly switch the field to a perpendicular angle. Both disassembly methods were used interchangeably. The distance between individual cuboids after separation was stochastic and was influenced by surface friction between the cuboid and the substrate. Partial separation could also occur from the disassembly methods due to surface friction or from geometric irregularities present along the surfaces of the cuboids. The effects of magnetic field magnitude on assembly and disassembly were not studied in detail; instead, only the maximum magnetic field produced by a single pair of coils was used (approximately 40 mT).

D. Motion Modes

Two motion modes were used to propel 'assembled cuboids'. The first motion mode is defined as 'rolling', where magnetic fields are iterated around the rotation axis (dashed line, Fig. 2e). The control algorithm to achieve rolling towards an arbitrary direction θ is described by **Algorithm 1**, where itr is the number of sequences performed and $delay$ is the pause time in seconds between each step. The second motion mode, known as 'pivot walking', involves pivoting one end of the assembled cuboids towards the workspace surface while lifting the other end off and swinging the lifted end with the applied magnetic torque about the x-y plane. The control algorithm for pivot walking perpendicular to an arbitrary angle θ is described by **Algorithm 2**; where the initial sign of the offset angle θ_1 is user selected and determines whether the robot pivot walks forwards $(+)$ or backwards $(-)$. The *delay* time in both algorithms was user modulated between 0.1 to 1 seconds while the number of iterations (*itr*) was also changed as needed. The pivot walking mode required larger iterations to achieve the same displacement as the rolling mode. However, the pivot walking mode was more flexible for larger assemblies of cuboids (see results).

Algorithm 1: Rolling towards θ

itr = 2;
delay = 0.2;
for *i:= 1* $\rightarrow itr$ **do**
  $\boldsymbol{B}_G$*(A,θ,0);*
  pause(delay);
  $\boldsymbol{B}_G$*(A,θ,-π/2);*
  pause(delay);
  $\boldsymbol{B}_G$*(A,θ-π,0);*
  pause(delay);
  $\boldsymbol{B}_G$*(A,θ-π,π/2);*
  pause(delay);

III. Results

A. Assembly and Disassembly

Assembly and disassembly of cuboid swarms largely followed the schematic presented previously in Fig. 2, with an example of assembly/disassembly in Fig. 3a-d between three cuboids; these three cuboids were manually placed in proximity to one another. The cuboids were found to repel when the magnetic field was pointed to the positive z axis and attract when pointed to the positive x direction where a combined cuboid was then formed. Separation of individual cuboids was found to occur in a reversal of the original sequence; where the magnetic field was switched along the negative x axis with the magnetic field, then being pointed to the positive z axis again to force the individual cuboids to magnetically repel each other. Applying a magnetic field along the positive y direction caused the cuboids to assemble laterally. This process, however, could be interfered with if geometric irregularities inherent to the cuboids or substrate caused non-uniform and stochastic separation behavior, as can be seen by the slight angle of the green cuboid in Fig. 3c.

B. Velocity and Pathing

Propelling individual cuboids meaningfully under static or rotating magnetic fields was not possible, although small position changes from the reorientation of the embedded magnets could cause cuboids to move towards one another if they were close enough together. While acceptable in some cases to help cuboids assemble, this form of propulsion was not ideal for highly controlled maneuvering. Instead, if two cuboids were assembled together as in Fig. 2c, the connected dipoles of the pair fix the two cuboids together and allow for body reorientation with the magnetic field (Fig. 2e). As an example, by setting θ to $3\pi/2$ and using **Algorithm**

Algorithm 2: Pivot walking perpendicular to θ

itr = 2;
delay = 0.2;
$\theta_1 = \pm 20\pi/180$;
$\alpha = 9\pi/180$;
for *i:= 1* $\rightarrow itr$ **do**
  $\boldsymbol{B}_G$*(A,θ+*θ_1*,*α*);*
  pause(delay);
  $\boldsymbol{B}_G$*(A,θ+*θ_1*,-*α*);*
  pause(delay);
  $\boldsymbol{B}_G$*(A,θ-*θ_1*,-*α*);*
  pause(delay);
  $\boldsymbol{B}_G$*(A,θ-*θ_1*,*α*);*
  pause(delay);

1, an assembled cuboid could be made to roll down the negative y axis. Figure 4a-f shows an example of this behavior whereby swarms of cuboids (4 total) were assembled together, reoriented along the negative y direction, rolled to the middle of the working area about the x axis, reoriented to face length-wise along the y axis, and then disassembled back into individual cuboids using the disassembly method. While both assembled cuboids experienced the same field inputs, stochastic differences between them (friction, incorrect dipole orientation, partial separation) created the non-uniform behavior exhibited in Fig. 4d, whereas the leftward assembled cuboid traveled further than the one on the right.

In general, most cuboids could behave reliably once assembled together and could propel either using the rolling mode or the pivot walking mode. To verify repeatability of their performance, both motion modes were performed using different delay times. Both the velocity and the displacement profiles were extracted from the motion of assembled cuboids under both motion modes, at four different delay times (0.1, 0.2, 0.5, and 1 seconds), and collected over at least four trials

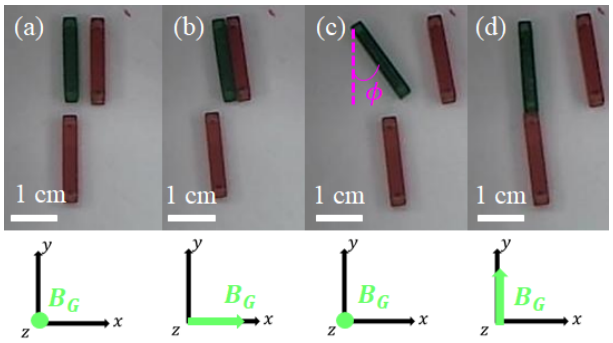

Fig. 3. (a) Cuboids were disassembled with the magnetic field pointing in the positive z direction, (b) assembled side-wise with a magnetic field in the positive x direction, (c) disassembled using the disassembly procedure, (d) assembled length-wise with a magnetic field pointed to the positive y-direction. Beneath each sub-figure shows the direction of the magnetic field ($\boldsymbol{B}_G$) along the plane. The offset angle ϕ in (c) was approximately 33° after disassembly. Magnetic field magnitude was approximately 40 mT.

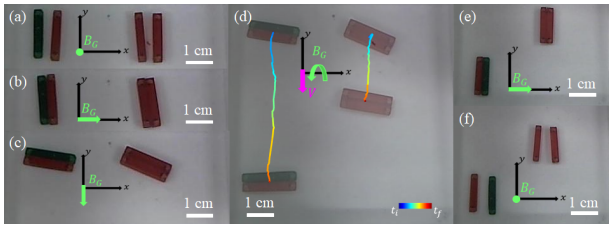

Fig. 4. (a) Four cuboid robots were placed within the workspace while the magnetic field was oriented to the positive z direction. (b) The magnetic field was switched to the positive x direction where two assembled cuboids were formed. (c) The assembled cuboids were reoriented when the magnetic field pointed along the negative y direction. (d) A counterclockwise rotation about the x axis caused the assembled cuboids to roll down the working space for 2 seconds. (e) Cuboids were reoriented when the magnetic field pointed in the positive x direction. (f) The assembled cuboids were separated into individual cuboids when the magnetic field was sequentially applied along the negative x direction and then along the positive z direction using the disassembly procedure. Green arrows represent the direction of the magnetic field ($\boldsymbol{B}_G$) and the magenta arrow shows the velocity direction ($\boldsymbol{V}$).

for each delay time. The results of these studies are shown in Fig. 5, where 5a and 5b are for the rolling motion mode, and 5c and 5d are for the pivot walking motion mode.

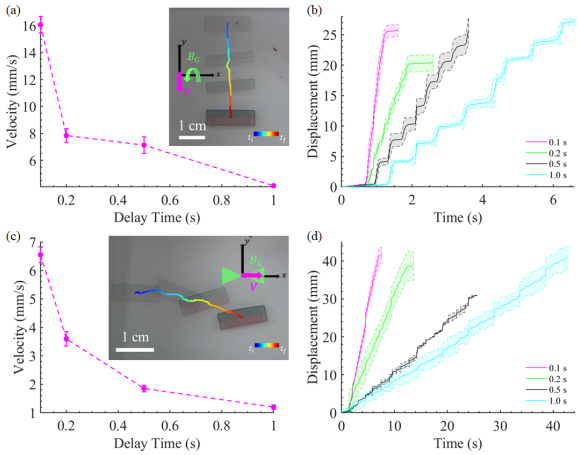

Fig. 5. (a) Velocity vs. delay time and (b) displacement vs. time for assembled cuboids performing 2 iterations of the rolling motion. (c) Velocity vs. delay time and (d) displacement vs. time for assembled cuboids performing pivot walking over 20 iterations. Shaded areas represent the bounds of the standard deviation over multiple trials. Insets in (a) and (c) show examples of each motion mode. Dashed lines in (a) and (c) were added as eye guides. Green arrows in the insets represent the direction of the magnetic field ($\boldsymbol{B}_G$) and the magenta arrow shows the velocity direction ($\boldsymbol{V}$).

As expected, under both motion modes, the smaller the delay time, the faster the assembled cuboids could propel. However, too fast a delay time (less than 0.05 seconds) was found to cause the rapid disassembly of assembled cuboids, most likely because the magnetic fields were cycling faster than the time required for the dipoles to properly align with them. The displacement achieved during repeated trials of both motion modes were also markedly similar as evidenced by Fig. 5b and 5d, with a very little standard deviation for each delay time. It is also important to note that while the rolling mode was almost twice as fast as the pivot walking mode at each delay time, both modes are situationally useful and can be switched between as required. An example of an assembled cuboid performing a square trajectory under both modes is seen in Fig. 6a and 6c; this demonstrates that the assembled cuboids are not limited to unidirectional control. The moving averaged velocity in Fig. 6b and 6d show how velocity changes over time when performing each segment of the square trajectory; both experiments had delay times of 0.1 seconds, with the iterations for rolling and pivot walking being 2 and 15 respectively, for each direction. While the rolling mode is relatively cyclical and almost perfectly square, the pivot walking mode was subject to far more variations both in displacement and velocity.

C. Object Transportation

To enable object transportation, the cuboid geometry was modified to contain a curved notch. The notch was large enough such that when two 'trap robots' were assembled, they could 'trap' any arbitrary object between them. In this

situation, the rolling motion mode shown previously was not effective since the geometry was too large laterally to roll; however, the pivot walking could still be easily implemented without any significant hindrances. Thus, after trapping an object, the trap robot could transport the payload to an arbitrary position and release it using the disassembly method. To demonstrate this ability, a 3D printed cube ($4 \times 4 \times 4\ mm^3$) was placed between two trap robots (Fig. 7a). Using a magnetic field along the y direction, the robots could be assembled together to encapsulate the cube (Fig. 7b). Using the pivot walking mode, the assembled robots could transport the cube across the working space to an arbitrary end position (Fig. 7c). Once the final position was reached, the disassembly method was utilized to separate the trap robots and release the payload (Fig 7d). Object manipulation was not limited to unidirectional motion only, as in Fig. 7e, the same cube was transported in a guided path around a much larger working area. The smoothed velocity profiles during this 2D motion are plotted in Fig. 7f with the color bar along the horizontal axis corresponding to the colored path in Fig. 7e. While the velocity profile is erratic at points, the velocities achieved correspond closely to those presented previously in Fig. 5c for a pivot walking cuboid at a delay time of 0.1 seconds.

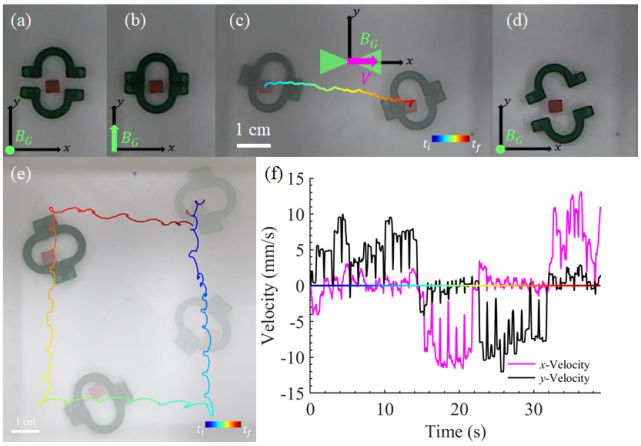

Fig. 7. (a) Trap robots were positioned around a cube shaped payload. (b) Using a magnetic field in the y direction, the trap robots were assembled. (c) The trap robots were moved across the working space using the pivot walking mode for 7 seconds. (d) The trap robots were separated using the disassembly method. (e) Assembled trap robots transporting a red 3D printed cube around the working space using pivot walking motion. Snapshots of the assembled trap robots were blended into the image to show progression. The total time of the experiment was 40 seconds. (f) Velocity components of the trap robot vs. time. Component velocities were smoothed using a moving average with a sliding window of 30 frames. Color bar in (e) corresponds to horizontal line in (f). Green arrows and shades represent the direction of the magnetic field ($\boldsymbol{B}_G$) and the magenta arrow shows the velocity direction ($\boldsymbol{V}$). Delay time and iterations for (c) were 0.1 seconds and 15, respectively.

D. Patterning and Templating

As shown in the previous section, adjusting the geometry of the cuboids could allow for very useful applications, such as object transportation, but modifying the geometry further could also enable the selective assembly and disassembly between certain cuboids. This allows cuboid templating to take place, whereby specific cuboid pairs will merge together while other pairs remain separate. The cuboids presented in Fig. 8a-d consisted of two male cuboids with five protrusions each, and one female cuboid, with five slots on each side, that were manually placed in the positions shown in Fig. 8a while a magnetic field was present along the positive z direction to prevent attachment. The idea here was that the five extrusions should fit perfectly with the female counterpart since both are evenly spaced. When a magnetic field was applied to the positive y direction (Fig. 8b), the upper and middle cuboids were assembled, while the vertical male cuboid remained stationary. The assembled cuboid was then actuated along the negative y direction using pivot walking motion (Fig. 8c), became attached to the stationary male cuboid, and then continued to move down the working space. Once the final destination was reached, the disassembly technique was utilized to separate the cuboids (Fig. 8d). To demonstrate further that protrusion and slot spacing could affect assembly of cuboids, two sets of cuboids were tested; the first set had the same cuboids as shown in Fig. 8a, but they were placed vertically to each other initially (Fig. 8e) with a magnetic field in the positive z direction. When the magnetic field was directed along the positive x direction, the three cuboids assembled together perfectly (Fig. 8f). When the same female cuboid (5 slots) was placed in proximity to two male cuboids with only four protrusions, that were differently spaced (Fig. 8g), the same experiment shows that after the magnetic field was applied along the positive x direction, only a partial assembly between the cuboids occurred (Fig. 8h). While factors such as friction and different initial conditions could

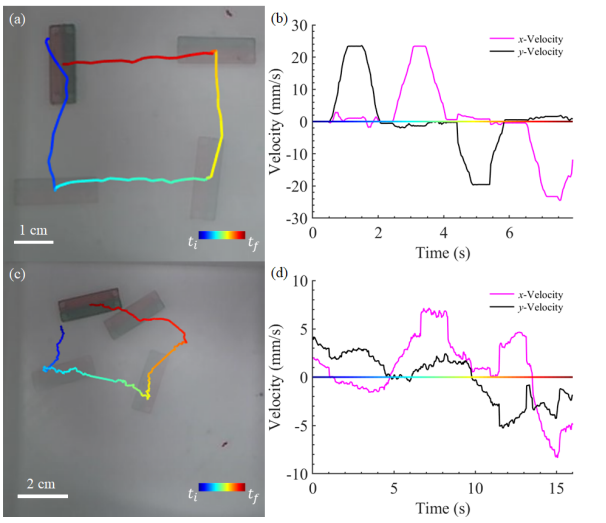

Fig. 6. (a) Path of an assembled cuboid performing a box motion by rolling. (b) Velocity components of the assembled cuboid vs. time. Component velocities were smoothed using a moving average with a sliding window of 30 frames. (c) Path of an assembled cuboid performing a box motion by pivot walking. (d) Velocity components of the assembled cuboid vs. time. Component velocities were smoothed using a moving average with a sliding window of 30 frames. Color bar in (a) corresponds to horizontal line in (b); same for the color bars shown in (c) and (d). The delay time for both experiments was 0.1 seconds, while the iterations for (a) and (c) during each segment of the square were 2 and 15, respectively.

also impede the assembly of both sets of cuboids, it was clear that the different protrusion and slot spacing of the cuboids in Fig. 8g-h hindered this assembly process significantly. Under partial assembly neither the pivot walking motion mode, shown previously in Fig. 8c, nor the rolling mode were achievable.

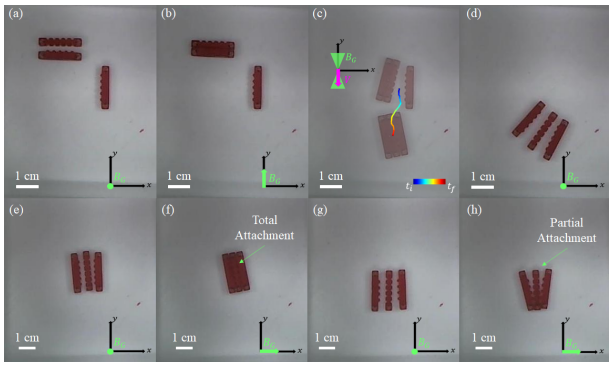

Fig. 8. (a) Cuboids with male and female geometries were positioned apart. (b) Two cuboids were assembled together using a magnetic field in the positive y direction. (c) As the assembled cuboids moved downward using the pivot walking motion mode, they became attached to a third cuboid and actuated across the working space; the total time of propulsion was approximately 10 seconds. (d) After reaching the target destination, the disassembly method was used, and the cuboids were separated. (e) Cuboids with mating male and female connections (5 protrusions, 5 slots) were positioned in proximity to one another with a magnetic field along the positive z direction. (f) When the magnetic field was reoriented along the positive x direction, the three cuboids became fully assembled together. (g) Cuboids with different non-mating connections (4 protrusions, 5 slots) were positioned in proximity to one another with a magnetic field along the positive z direction. (h) When the magnetic field was reoriented along the positive x direction, the three cuboids only be partially assembled together. Green arrows and shades represent the direction of the magnetic field ($\boldsymbol{B}_G$) and the magenta arrow shows the velocity direction ($\boldsymbol{V}$). Delay time and iterations for (c) were 0.1 seconds and 20, respectively.

IV. Conclusions

The dexterity, adaptability, and versatility of wirelessly controlled cuboids was demonstrated. Simple in design and easy to fabricate, cuboids successfully demonstrated a high degree of repeatable and predictable responses to pre-planned field inputs, allowing for both the controllable assembly of individual cuboids and their propulsion using either rolling or pivot walking motion modes. Stochastic effects, produced from surface friction and fabrication deficiencies, could greatly impact the propulsion of assembled cuboids and interfere with their assembly processes. Assembled cuboids displayed high degrees of predictable velocities and displacements under fixed delay times and iterations. While the rolling mode was faster than the pivot walking mode, the pivot walking mode was found to be more useful in applications that involved payload transportation and applications that involved templating cuboids together.

While the results presented here only show one size of permanent magnets, smaller permanent magnets, as well as ferromagnetic microparticles, are available and can be used with highly precise microfabrication techniques (two photon 3D printers) to create smaller versions of these cuboid robots. Similar microscale designs have already been produced in work by Alapan et al. [26], where dielectric forces were used to attract microparticles to SU-8 structures and create novel microrobotic vehicles. These same dielectric forces could be used to fabricate cuboids, while super imposed magnetic fields could be used in tandem for assembly and actuation. We intend to develop this in future work as well as investigate feedback control and create automated assembly/disassembly procedures that can produce useful assemblies using the cuboids as subunits.

Appendix

Readers are encouraged to view the supporting information video included with this manuscript. The video includes demonstrations of the assembly, disassembly, rolling, pivot walking, object transport, and templating experiments discussed here.

Acknowledgment

We would like to thank Micah Oxner for helping with preliminary investigations. This work was supported by the National Science Foundation (CMMI #1712096, CMMI #1760642 & IIS #1712088).

References

[1] J. Liu, X. Zhang, and G. Hao, "Survey on research and development of reconfigurable modular robots," *Advances in Mechanical Engineering*, vol. 8, no. 8, pp. 1–21, 2016.

[2] M. Yim, W.-M. Shen, B. Salemi, D. Rus, M. Moll, H. Lipson, E. Klavins, and G. S. Chirikjian, "Modular self-reconfigurable robot systems [grand challenges of robotics]," *IEEE Robotics & Automation Magazine*, vol. 14, no. 1, pp. 43–52, 2007.

[3] U. A. Fiaz and J. S. Shamma, "usbot: A modular robotic testbed for programmable self-assembly," *IFAC-PapersOnLine*, vol. 52, no. 15, pp. 121–126, 2019.

[4] K. Gilpin, K. Kotay, D. Rus, and I. Vasilescu, "Miche: Modular shape formation by self-disassembly," *The International Journal of Robotics Research*, vol. 27, no. 3-4, pp. 345–372, 2008.

[5] P. Moubarak and P. Ben-Tzvi, "Modular and reconfigurable mobile robotics," *Robotics and Autonomous Systems*, vol. 60, no. 12, pp. 1648–1663, 2012.

[6] W. Saab, P. Racioppo, and P. Ben-Tzvi, "A review of coupling mechanism designs for modular reconfigurable robots," *Robotica*, vol. 37, no. 2, pp. 378–403, 2019.

[7] S. Murata, E. Yoshida, A. Kamimura, H. Kurokawa, K. Tomita, and S. Kokaji, "M-tran: Self-reconfigurable modular robotic system," *IEEE/ASME Transactions on Mechatronics*, vol. 7, no. 4, pp. 431–441, 2002.

[8] J. Lengiewicz and P. Hołobut, "Efficient collective shape shifting and locomotion of massively-modular robotic structures," *Autonomous Robots*, vol. 43, no. 1, pp. 97–122, 2019.

[9] M. Rubenstein, A. Cornejo, and R. Nagpal, "Programmable self-assembly in a thousand-robot swarm," *Science*, vol. 345, no. 6198, pp. 795–799, 2014.

[10] Z. Butler, K. Kotay, D. Rus, and K. Tomita, "Generic decentralized control for lattice-based self-reconfigurable robots," *The International Journal of Robotics Research*, vol. 23, no. 9, pp. 919–937, 2004.

[11] J. Y. Kim, T. Colaco, Z. Kashino, G. Nejat, and B. Benhabib, "mroberto: A modular millirobot for swarm-behavior studies," in *2016 IEEE/RSJ International Conference on Intelligent Robots and Systems (IROS)*, pp. 2109–2114, Daejeon, South Korea, 2016.

[12] Y. Li, S. Zhu, Z. Wang, L. Zhang, X. Ma, and Z. Cui, "The kinematics analysis of a novel self-reconfigurable modular robot based on screw theory," *DEStech Transactions on Engineering and Technology Research*, 2016.

[13] H. Mabed and J. Bourgeois, "Scalable distributed protocol for modular micro-robots network reorganization," *IEEE Internet of Things Journal*, vol. 3, no. 6, pp. 1070–1083, 2016.

[14] J. Bishop, S. Burden, E. Klavins, R. Kreisberg, W. Malone, N. Napp, and T. Nguyen, "Programmable parts: A demonstration of the grammatical approach to self-organization," in *2005 IEEE/RSJ International Conference on Intelligent Robots and Systems*, pp. 3684–3691, Edmonton, Alberta, Canada, 2005.

[15] M. Sitti, H. Ceylan, W. Hu, J. Giltinan, M. Turan, S. Yim, and E. Diller, "Biomedical applications of untethered mobile milli/microrobots," *Proceedings of the IEEE*, vol. 103, no. 2, pp. 205–224, 2015.

[16] R. Pfeifer, M. Lungarella, and F. Iida, "Self-organization, embodiment, and biologically inspired robotics," *Science*, vol. 318, no. 5853, pp. 1088–1093, 2007.

[17] P. J. White and M. Yim, "Scalable modular self-reconfigurable robots using external actuation," in *2007 IEEE/RSJ International Conference on Intelligent Robots and Systems*, pp. 2773–2778, San Diego, CA, U.S.A., 2007.

[18] E. Diller, C. Pawashe, S. Floyd, and M. Sitti, "Assembly and disassembly of magnetic mobile micro-robots towards deterministic 2-d reconfigurable micro-systems," *The International Journal of Robotics Research*, vol. 30, no. 14, pp. 1667–1680, 2011.

[19] S. Miyashita, E. Diller, and M. Sitti, "Two-dimensional magnetic micro-module reconfigurations based on inter-modular interactions," *The International Journal of Robotics Research*, vol. 32, no. 5, pp. 591–613, 2013.

[20] H. Gu, Q. Boehler, D. Ahmed, and B. J. Nelson, "Magnetic quadrupole assemblies with arbitrary shapes and magnetizations," *Science Robotics*, vol. 4, no. 35, 2019.

[21] U. K. Cheang, F. Meshkati, H. Kim, K. Lee, H. C. Fu, and M. J. Kim, "Versatile microrobotics using simple modular subunits," *Scientific Reports*, vol. 6, p. 30472, 2016.

[22] X. Dong and M. Sitti, "Controlling two-dimensional collective formation and cooperative behavior of magnetic microrobot swarms," *The International Journal of Robotics Research*, in press, 2020.

[23] H. Xie, M. Sun, X. Fan, Z. Lin, W. Chen, L. Wang, L. Dong, and Q. He, "Reconfigurable magnetic microrobot swarm: Multimode transformation, locomotion, and manipulation," *Science Robotics*, vol. 4, no. 28, p. eaav8006, 2019.

[24] L. Ferranti and F. Cuomo, "Nano-wireless communications for microrobotics: An algorithm to connect networks of microrobots," *Nano Communication Networks*, vol. 12, pp. 53–62, 2017.

[25] E. A. Khatib, A. Bhattacharjee, P. Razzaghi, L. W. Rogowski, M. J. Kim, and Y. Hurmuzlu, "Magnetically actuated simple millirobots for complex navigation and modular assembly," *IEEE Robotics and Automation Letters*, vol. 5, no. 2, pp. 2958–2965, 2020.

[26] Y. Alapan, B. Yigit, O. Beker, A. F. Demirörs, and M. Sitti, "Shape-encoded dynamic assembly of mobile micromachines," *Nature Materials*, vol. 18, pp. 1244–1251, 2019.